8

Design and Analysis of Key Components in the Nanoindentation and Scratch Test Device

Hongwei Zhao, Hu Huang, Jiabin Ji and Zhichao Ma
Jilin University
China

1. Introduction

In recent years, nanomechanics as an important branch of nanotechnology has been an effective method to study mechanical properties of structures and materials from micro- to nano-scale. It has been widely used to study mechanical behaviour and damage mechanism of nanotube, nanobelt as well as other nanostructures (Zhu & Espinosa, 2005; Han et al., 2007). Some researchers studied biomechanics properties of tissues and organs of human body, such as the red cell (Suresh, 2007; Lim et al., 2006) and bone (Tai et al., 2007; Hansma et al., 2006; Thurner, 2009; Zheng & Mak, 1996; Koff et al., 2010; Huja et al., 2010; Diez-Perez et al., 2010; Zhang et al., 2010) by means of experimental nanomechanics approaches, to reveal occurrence rules, prevention and control methods of some diseases.

Compared with tensile, torsion, bend and hardness tests etc. during which samples are usually in condition of simple stress state, nanoindentation and scratch test can obtain more parameters of materials including hardness, modulus, fracture toughness, creep property, fatigue, adhesion and so on (Doerner & Nix, 1986; Oliver & Pharr, 1992) because samples are in condition of complex stress state. So, it has been widely used in fields of materials science (Lucas & Oliver, 1999; Yang et al., 2007; Tao et al., 2010), nanotechnology, surface engineering (Jardret & Morel, 2003), semiconductor (Michler et al., 2005; Zhao et al., 2009), MEMS/NEMS (Abdel-Aal et al., 2005; Bhushan, 2007), biomedicine (Suresh, 2005), biomechanics (Bruet et al., 2008) and so on. In addition, it is a useful method to study multi-physical field coupled performance of materials (Bradby et al., 2003; Schuh et al., 2005; Nowak et al., 2009). So in past years, nanoindentation and scratch test gave a big boost to the development of related fields and also it was given huge attention in all over the world.

With further development of materials science and nanomechanics, more and more researchers tried to study principle of deformation and damage of materials (De Hosson et al., 2006; Rabe, 2006; Zhou & Komvopoulos, 2006). Nanoscale deformation: Seeing is believing (Hemker & Nix, 2008). So research on in situ nanoindentation and scratch test was proposed, through which process of deformation and damage of samples can be observed. However, because of large size and complex structure of existing commercial equipments (MTS NanoIndenter; Hysitron Incorporated; CSIRO.UMIS; Micro Materials Ltd.; CSM instruments), they can not be installed on the stage of SEM or TEM to realize in situ nanoindentation and scratch test. So, novel nanoindentation and scratch test devices are required. And this is advanced technology and up to now there is no mature product for in situ nanoindentation and scratch test.

In this chapter, we introduced principle of nanoindentation. A new method of indentation measurement through two displacement sensors and a displacement amplification structure was proposed. This measuring method was different from many commercial devices. Two key components of the proposed device including precise driving and precise measuring units were designed and analyzed. Hysteresis of two kinds of piezoelectric stacks were measured and analyzed. Here piezoelectric stacks and flexure hinges were used to realize precise positioning and precise loading and unloading of the diamond indenter. Flexure hinges with multi-structure forms were proposed and analyzed by finite element method. Based on the previous work, the prototype of nanoindentation and scratch device was designed and fabricated. Calibration experiments of sensors and displacement amplification structure were carried out and output performances of designed flexure hinges were measured and discussed. At last, nanoindentation experiments of optical glass were carried out. The relation curves between penetration load and depth were obtained, from which hardness of the glass was figured out. Nanoindentation morphology was obtained through high resolution optical microscope. Nanoindentation results indicated that the device presented in this chapter can realize the high precise nanoindentation test, but the testing resolution should be improved and the device also should be calibrated precisely. Though the accuracy was required to improve, this work was a bold attempt to combine the piezoelectric-driven mechanism and flexure hinge to realize precise motion in nanoindentation device. This transmission mode is very simple and can be used easily to realize miniaturization of the device and in situ nanoindentation test which is our future work.

2. Principle of nanoindentation test technology---the Oliver-Pharr method

Nanoindentation is a useful method to test the mechanical behavior and damage mechanism of materials from micro- to nano-scale. When a diamond indenter with sharp tip is penetrating into and then withdrawing from a sample surface, the load P and displacement h is continuously monitored by high resolution sensors. The load and displacement data is sent to processor during the indentation process and then converted to P-h curve which contains abundant information of material such as hardness, elastic modulus, yield stress and so on. Fig.1 is a typical P-h curve of nanoindentation. It mainly

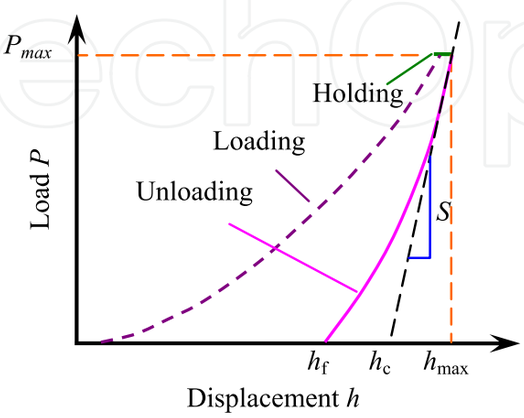

Fig. 1. A typical P-h curve of nanoindentation

consists of two portions, loading and unloading process. Sometimes, in order to study creep of materials, holding portion (holding for a certain time at maximum load) between loading and unloading is added. Fig.2 is cross-section of indentation and the related parameters. Up to now, the Oliver-Pharr method (Oliver & Pharr, 1992) based on results by Sneddon (Sneddon, 1965) is most commonly used to analyze the load and penetration depth for nanoindentation measurements.

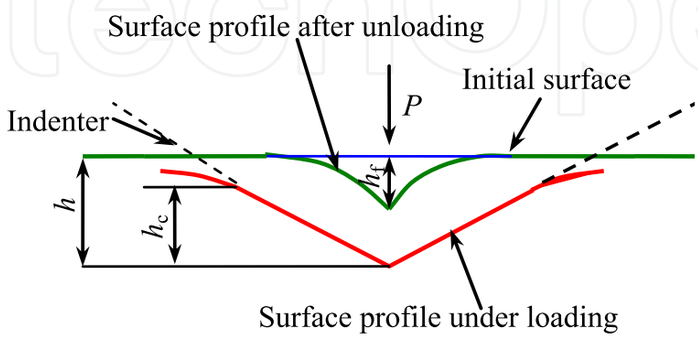

Fig. 2. Cross-section of indentation

According to Oliver-Pharr method, nanoindentation hardness is defined as the indentation load divided by the projected contact area of the indentation. In Fig.1, indentation hardness (H) can be obtained at the peak load given by

$$H = P_{\max}/A_c \tag{1}$$

where $P_{\max}$ is the peak load and A_c is the projected contact area. And the projected contact area can be calculated from the relation as following

$$A_c = f(h_c) \tag{2}$$

where h_c is the contact depth which is given by

$$h_c = h_{\max} - \varepsilon \frac{P_{\max}}{S} \tag{3}$$

where ε is a constant and depends on the geometry of the indenter (ε=0.72 for cone indenter, ε=0.75 for paraboloid of revolution, and ε=1.00 for flat indenter) (Sneddon, 1965). $h_{\max}$ is the maximum penetration depth and S is the contact stiffness.

The contact stiffness S can be calculated from the slope of the initial portion of the unloading curve and $S=dP/dh$, which can be obtained by curve fitting of 25%-50% unloading data.

Based on relationships developed by Sneddon, the contact stiffness S can also be expressed by

$$S = 2\beta\sqrt{\frac{A}{\pi}}E_r \tag{4}$$

where β is a constant and depends on geometry of the indenter (β =1.034 for a Berkovich indenter, β =1.012 for a Vickers indenter and β =1.000 for a cylinder indenter).
Because both the sample and the indenter have elastic deformation during the indentation process, the reduced modulus E_r is defined by

$$\frac{1}{E_r} = \frac{1-\nu^2}{E} + \frac{1-\nu_i^2}{E_i} \tag{5}$$

where E and ν are the elastic modulus and Poisson's ratio for the sample; E_i and ν_i are the elastic modulus and Poisson's ratio for the indenter, respectively. For a diamond indenter, E_i =1141GPa, ν_i =0.07.
According to the Oliver-Pharr method mentioned above, the nanoindentation hardness, the contact stiffness and the elastic modulus of materials can be obtained.

3. Idea of device design

Fig.3 is the schematic diagram of indentation device which will be designed in this chapter. It mainly consists of two portions, precise driving unit including z-axis precise driving unit (4), x, y precise positioning platform (8) and precise measuring unit including capacitance displacement sensor (5), displacement amplification structure (9) and laser displacement sensor (10). Compared with most of commercial indentation equipments, the principle is different. Penetration load is not measured directly by a load sensor but it is obtained with the help of displacement amplification structure and laser displacement sensor. When the indenter is pushing into and withdrawing the sample located on the left of displacement amplification structure, the amplification structure will deform and the right will output enlarged displacement which is measured by high resolution laser displacement sensor. At the same time, displacement of the indenter is measured by the capacitance displacement sensor. Because deformation of displacement amplification structure is very small, it is elastic deformation.

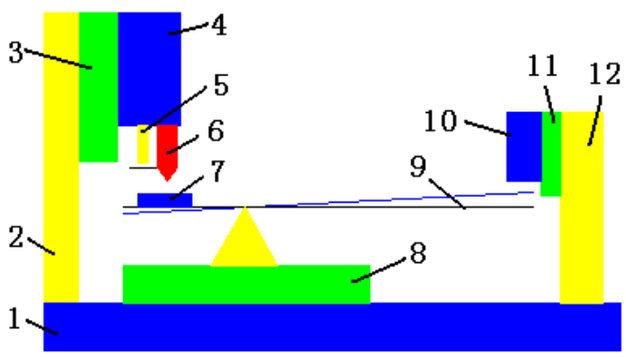

Fig. 3. Schematic diagram of the device which will be designed in this chapter 1 Base; 2(12) Supporting plates; 3(11) Macro-adjusting mechanism; 4 z-axis precise driving unit; 5 Capacitance displacement sensor; 6 Indenter; 7 Sample; 8 x, y precise positioning platform; 9 Displacement amplification structure; 10 Laser displacement sensor

Calculation model and related parameters are shown in Fig.4. P is penetration load and h_3 is left deformation of displacement amplification structure corresponding to the load P. h_1 and

h_2 are right deformation and displacement of the indenter measured by laser displacement sensor and capacitance displacement sensor, respectively. P, h_1, h_2, h_3 and penetration depth h have relationships as follows

$$h_3 = \mu h_1 \tag{6}$$

$$P = \lambda h_1 \tag{7}$$

$$h = h_2 - h_3 = h_2 - \mu h_1 \tag{8}$$

where μ and λ are calibration coefficients.

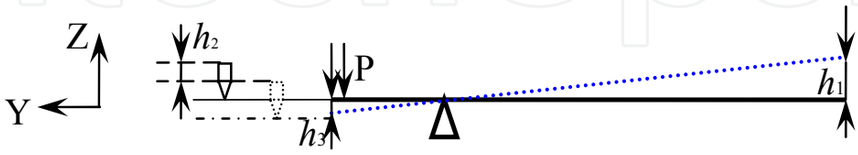

Fig. 4. Calculation model and the related parameters.

According to equations (6)—(8), penetration load P and depth h can be obtained, and material parameters can be calculated by the Oliver-Pharr method.

4. Design and analysis of precise driving units

Nanoindentation and scratch test technology mainly involves precise driving and precise measuring technology. For precise driving, there are many choices, for example, electromagnetic driver, shape memory alloy driver, micro-film, micro-beam and so on. Up to now, most of indentation devices are large because of using of electromagnetic and electrostatic drivers which also need complex control. Due to size limitation of SEM and TEM, these large indentation devices can not be used to realize in situ indentation test. So it is necessary to find more suitable driving mechanism to ensure miniaturization of indentation device. In this section, based on early research foundation on the piezoelectric-driven and flexure hinge, kinds of precise driving units realized by piezoelectric actuator and flexure hinge were designed.

4.1 Piezoelectric actuator

Principle of piezoelectric actuator is shown in Fig.5 which is based on the inverse piezo effect. The piezoelectric actuator will deform when an electric voltage signal is applied to it.

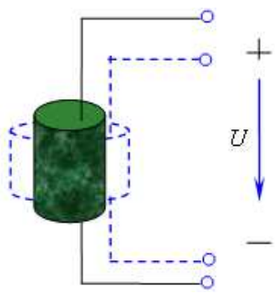

Fig. 5. Principle of piezoelectric actuator

The amount of movement is a function of the polarity of the voltage applied and the direction of the polarization vector.

Piezoelectric actuator takes many advantages of small size, unlimited resolution, large force generation, fast response, low power consumption and no wear. So it is widely used in fields of actuators, micro- and nano-positioning, laser tuning, active vibration damping, micropumps, and so on. In this chapter, two kinds of piezoelectric actuator are selected, PT200/10*10/40 piezoelectric stack used for z axis and AE0505D16F for x-y axis.

Hysteresis is an inherent property of piezoelectric ceramic. Hysteresis of the two kinds of piezoelectric stacks was measured and shown in Fig.6 and Fig.7.

In Fig.6 and Fig.7, there are two curves, respectively. One is the output displacement when voltage increases and the other is the output displacement when the voltage decreases. It is obvious that the displacement is different at the same voltage and the two curves are not symmetrical. The hysteresis H can be expressed

$$H = {}^{D_{DMAX}}\!/_{D_S} \times 100\% \tag{9}$$

where D_{DMAX} is the maximum difference of displacement at the same voltage; D_S is the total output displacement. In Fig.6, the maximum difference of displacement is about 1.15μm at voltage 45V and the total output displacement is 12.91μm. According to equation (9), the hysteresis is about 8.91% for AE0505D16F. In Fig.7, the maximum difference of displacement is about 5.49μm at voltage 45V and the total output displacement is 35.92μm. According to equation (9), the hysteresis is about 15.28% for PT200/10*10/40 piezoelectric stack. So hysteresis is different for different kinds of piezoelectric stacks and some measurements for example close-loop control should be taken to decrease the hysteresis for special application.

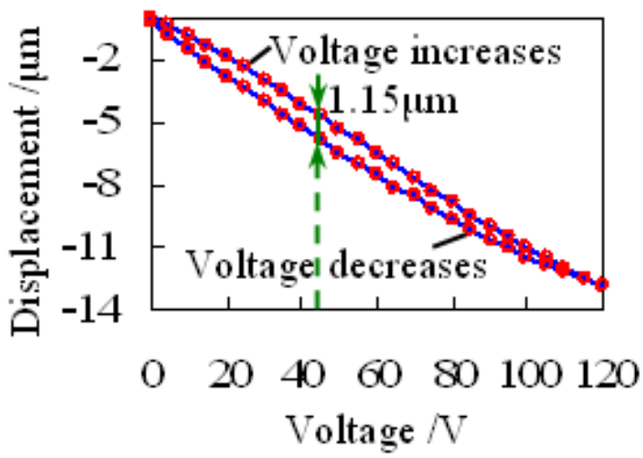

Fig. 6. Hysteresis curve of AE0505D16F

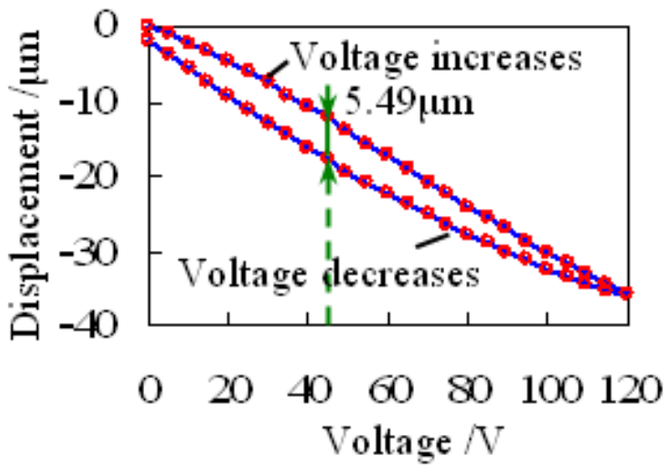

Fig. 7. Hysteresis curve of PT200/10*10/40

4.2 Flexure hinges

Materials and structures will deform under the external load and the deformation is usually very small and linear. Those are the working principle of flexure hinges. Compared to conventional mechanisms with sliding and rolling bearings, the flexure hinge takes many advantages of simple and compact structure, no lubrication and high positioning accuracy. For these reasons, flexure hinges have been widely used in fields of micro-positioning, micromanipulation, micro-gripper and so on.

Stiffness and output displacement of flexure hinges are contradictory to each other. Larger elastic deformation is hoped to ensure output displacement. On the other hand, enough stiffness is also very important to ensure the device having good dynamic characteristic and the anti-interference ability. Also internal stress of materials should not exceed permissible stress. Currently, there are four kinds of materials—beryllium bronze, aluminium, steel and titanium alloy to be used to fabricate flexure hinges. For these four kinds of materials, titanium alloy has the highest inherent frequency and best anti- interference ability, while the displacement is too small. In contrast, beryllium bronze has larger elastic deformation, but cost of these two kinds of materials is too high, and they are not suitable to make flexure hinges. Here, 65Mn was chosen to process them, which had numerous advantages of cheap price, high sensitivity, low elastic lag, high fatigue resistance, etc.

4.2.1 Z-axis flexure hinge

Z-axis precise driving unit consists of z-axis flexure hinge and z-axis piezoelectric actuator, and it is used to realize the precise loading and unloading of the indenter. Z-axis piezoelectric actuator was PT200/10*10/40 piezoelectric stack. Large output displacement

was given to z-axis flexure hinge realized by the level-type enlarging structure as shown in Fig.8, which was convenient to estimate the initial contact point.

Static and modal analysis was carried out to evaluate strength and dynamic performance of z-axis flexure hinge by finite element method. Displacement load of 10μm was applied to the area where piezoelectric actuator was located. And analysis results were shown in Fig.9 and Fig.10. As shown in Fig.9, displacement of 42μm was obtained at the output end which indicated that magnification of the flexure hinge was about 4, while the maximum stress was 33MPa, which was less than permissible stress of 65Mn being 432MPa. The first three natural frequencies of the flexure hinge were about 1133.7Hz、1366.7Hz、4243.5Hz which indicated that z-axis flexure hinge had good stability in the indentation device working at low frequency condition.

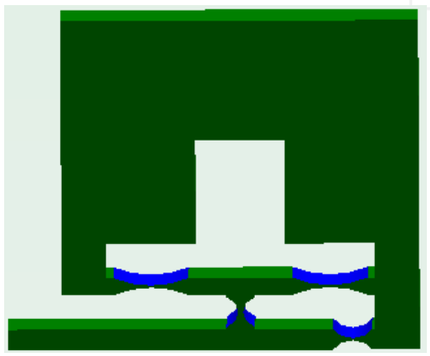

Fig. 8. Model of z-axis flexure hinge

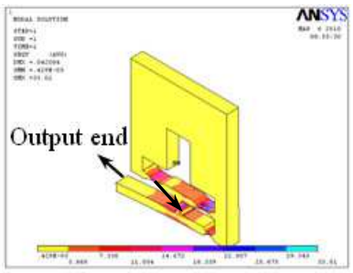

Fig. 9. Stress of z-axis flexure hinge

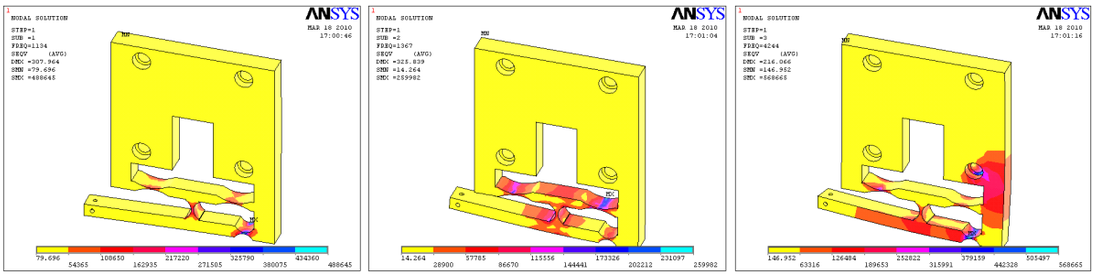

a) b) c)

Fig. 10. Mode shapes of z-axis flexure hinge (a) First mode shape (1133.7Hz); (b) Second mode shape (1366.7Hz); (c) Third mode shape (4243.5Hz)

4.2.2 x-y precise positioning hinge

x-y precise positioning platform including y-axis macro-adjusting mechanism, x-y precise positioning hinge and x-y piezoelectric actuators, is used to realize precise positioning of sample during indentation test and to realize precise motion of the sample during the scratch test. y-axis macro-adjusting mechanism as well as another two macro-adjusting mechanisms was bought directly and the models were GCM-1253001BM. x-y piezoelectric actuators were AE0505D16F piezoelectric stacks. The designed x-y precise positioning hinge was shown in Fig.11. Static and modal analysis results were shown in Fig.12 and Fig.13. The maximum stress was 158.6MPa, which was less than permissible stress of 65Mn being 432MPa. The first three natural frequencies of the flexure hinge were about 2669.5 Hz, 4831.0 Hz, 6281.8 Hz and the hinge had good dynamic performance.

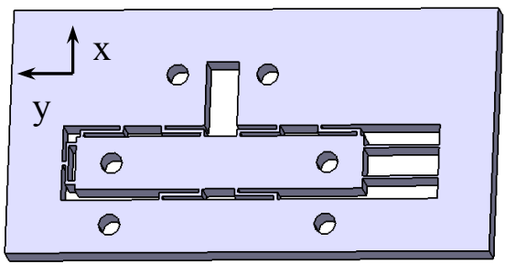

Fig. 11. Model of x-y precise positioning hinge

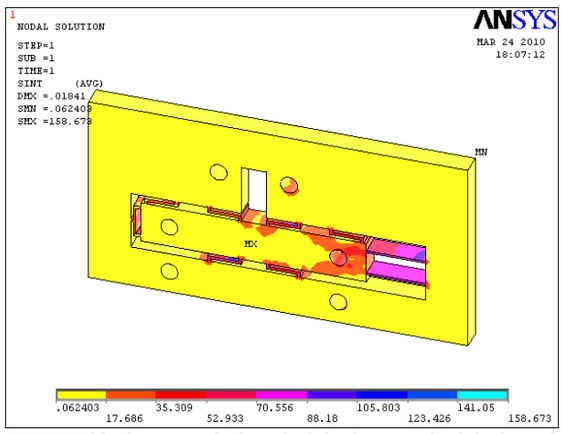

Fig. 12. Stress of x-y precise positioning hinge

5. Precise measuring unit

Parameters of materials are calculated by the penetration load and depth data. Because it is on very small scales, very high accuracy and resolution is required for sensors. As mentioned in section 3, penetration load and depth is obtained by indirect measurement method.

The displacement amplification structure and two displacement sensors are used to realize measurement. The laser displacement sensor LK-G10 which has resolution of 10nm is used to measure the output end (the right) of the displacement amplification structure, and the capacitance displacement sensor MDSL-0500M6-1 which has resolution of 10nm is used to

measure the displacement of the indenter. Then the measurement data is collected by the A/D card and sent to the computer. The main parameters of the two sensors are shown in table 1.

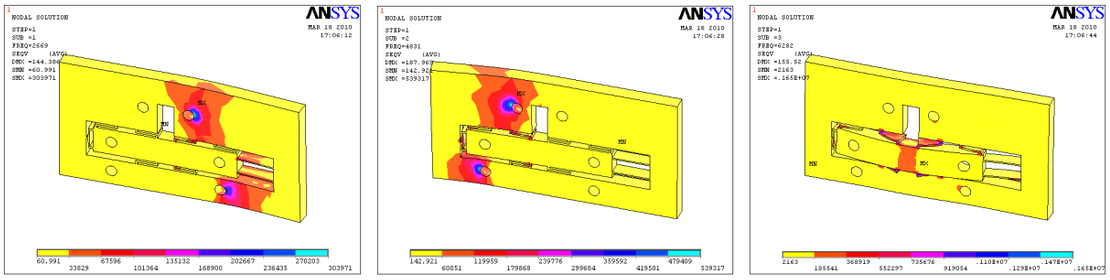

a) b) c)

Fig. 13. Mode shapes of x-y precise positioning hinge (a) First mode shape (2669.5Hz); (b) Second mode shape (4831.0Hz); (c) Third mode shape (6281.8Hz)

	LK-G10	MDSL-0500M6-1
Measurement range	±1mm	±0.5mm
Resolution	10nm	10nm
Accuracy	±0.02% F.S.	±0.02% F.S.
Reference distance	10mm	0mm
Linearity	±0.03% F.S.	±0.025% F.S.

Table 1. Main parameters of the two sensors

In this section, we will focus on design and analysis of the displacement amplification structure which plays an important role in measuring unit as well as entire indentation device. The designed displacement amplification structure with a lever amplification mechanism is shown in Fig.14. The sample is located on point A during the indentation test. Work principle is shown in Fig.15. Assumptions are as follows:

1. The upper thin plate rotates around the point O and the rotation angle is so small that the plate can be thought to be horizontal;
2. There is no bend deformation for the upper thin plate during the rotation.

Fig. 14. Model of amplification structure

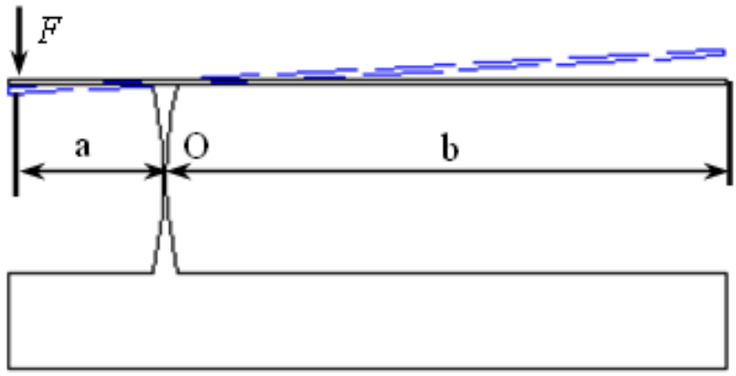

Fig. 15. Work principle of amplification structure

As shown in Fig.15, the displacement amplification structure not only works as a sample stage but also has the function of amplifying displacement signal. According to Fig.4 and Fig.15, the magnification factor is given by

$$k = \frac{|h_1|}{|h_3|} = \frac{b}{a} \tag{10}$$

where a is the horizontal distance between point A and the rotation point O; b is the horizontal distance between point B and the rotation point O.

In this chapter, the magnification factor k was designed to be 4. Static and modal analysis was carried out to evaluate the strength, output displacement and dynamic performance of displacement amplification structure. Displacement load of 10μm was applied to point A. Output displacement of point B was 38.2μm shown in Fig.16, and the maximum stress was 6.04MPa which was less than permissible stress of 65Mn being 432MPa. Fig.17 was the first three mode shapes and the first three natural frequencies were 170.53Hz, 407.42Hz, and 909.51Hz. The displacement amplification structure would bend or rotate at the structure' first three natural frequencies which were a little low. So the work frequency of the indentation device should be away from natural frequencies to avoid sympathetic vibration and also it is better to take measures to alleviate and isolate the vibration existing in the surroundings.

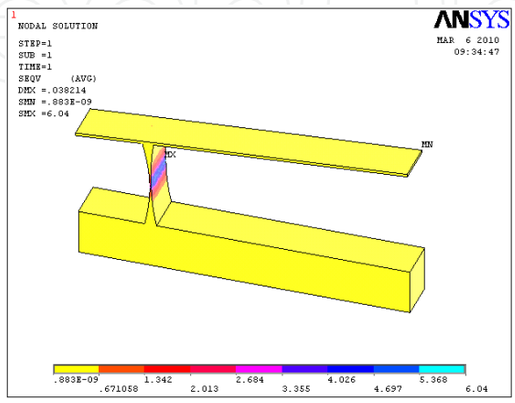

Fig. 16. Stress of amplification structure

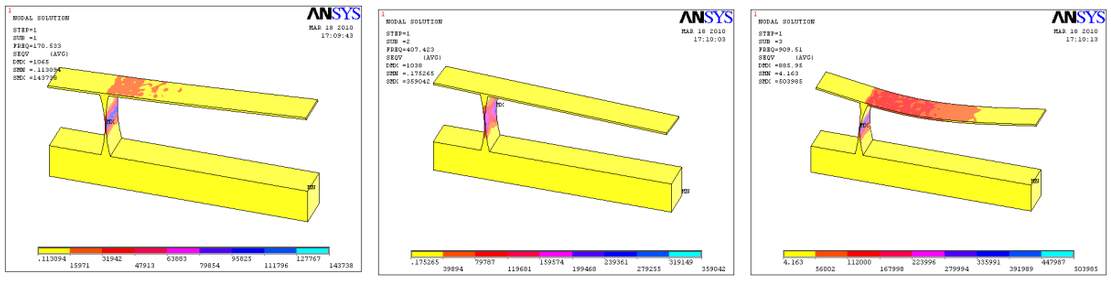

a) b) c)

Fig. 17. Mode shapes of displacement amplification structure (a) First mode shape (170.53Hz); (b) Second mode shape (407.42Hz); (c) Third mode shape (909.51Hz)

Output performances of the amplification structure under small load were analyzed by finite element method when the load *F* was 0.1mN and 1mN, respectively. Analysis results were shown in Fig.18 and Fig.19 respectively. In these two figures, the amplification structure had 43.3nm and 433nm output displacements corresponding to the loads 0.1mN and 1mN. The magnifications of input loads and output displacements were coincident which indicated that the structure had good linear output performance. Output displacement of 43.3nm can be detected easily by laser displacement sensor with the resolution of 10nm. That was to say the load resolution of the displacement amplification structure was higher than 0.1mN.

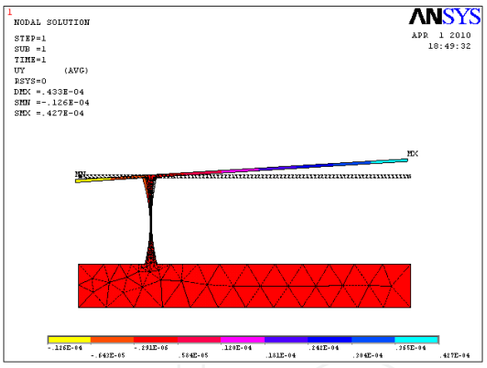

Fig. 18. Deformation of amplification structure when *F*=0.1mN

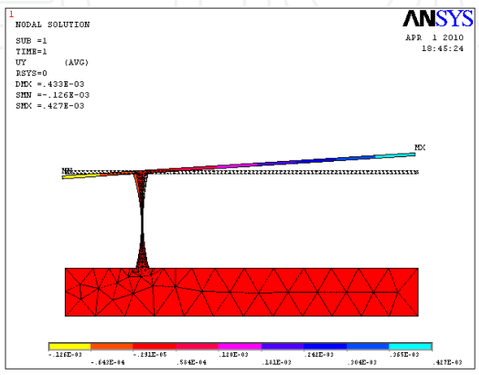

Fig. 19. Deformation of amplification structure when *F*=1mN

6. Prototype design

According to the analysis in the previous sections, the catia model of designed indentation device was shown in Fig.20. Parts were fabricated and the prototype was assembled as shown in Fig.21. The brief work processes are as follows:

1. Clear the sample surface;
2. Install the sample on the displacement amplification structure;
3. Install the indenter and lock it with the lock screw;
4. Adjust the macro-adjusting mechanism to make the laser displacement sensor in the suitable measuring range(the indicator light will be green);
5. Apply voltage to electronic components and wait for a moment to make the components stabilization;
6. Adjust the z-axis macro-adjusting mechanism to make the indenter close to the sample surface. When it is very close to the surface, stop macro-adjusting mechanism and apply voltage to the z-axis piezoelectric stack. Use the change of the read of the laser displacement sensor to judge the contact between the indenter and the sample surface;
7. Choose suitable voltage step to load and unload the indenter. During the process, use software to record the data sent by the A/D card. And then, process the data and obtain parameters of the sample.

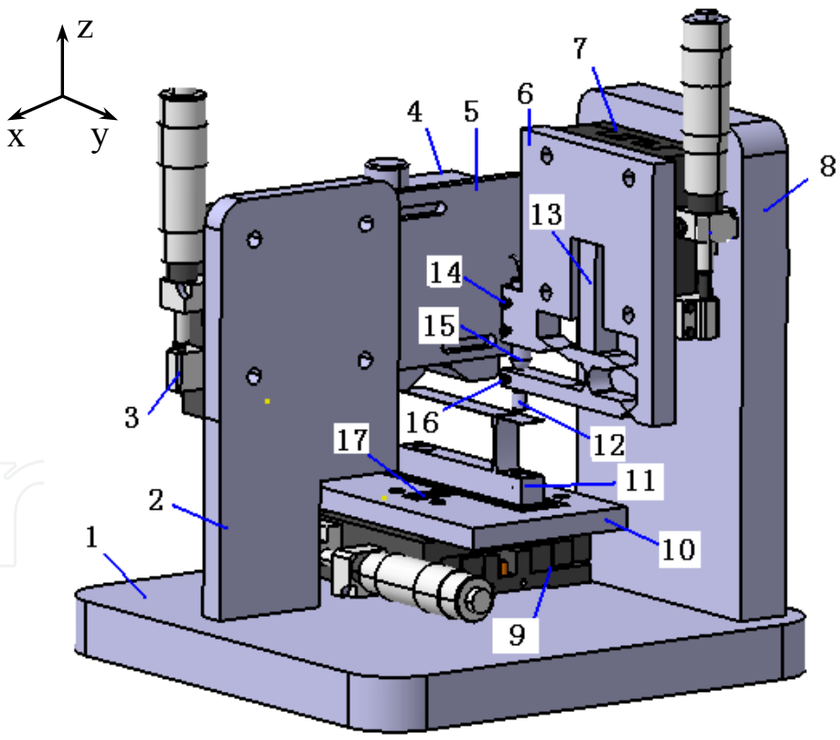

Fig. 20. Catia model of designed indentation device 1 Base; 2(8) Supporting plates; 3(7,9) Macro-adjusting mechanism; 4 Laser displacement sensor; 5 Connector; 6 z-axis flexure hinge; 10 x-y precise positioning hinge; 11 Displacement amplification structure; 12 Indenter; 13 z-axis piezoelectric stack; 14 Lock screws of the sensor ; 15 Capacitance displacement sensor; 16 Lock screw of the indenter; 17 x-axis piezoelectric stack.

Fig. 21. Prototype of designed indentation device

7. Experiments

In this section, experiments of the designed indentation device were carried out to evaluate its performances. These experiments mainly include calibration of laser and capacitance displacement sensors as well as the displacement amplification structure, output performance test of the designed x-y precise positioning hinge and z-axis precise driving hinge and indentation test of optical glass.

7.1 Calibration experiments of the sensors

Use z-axis precise driving unit to generate precise displacement signal. Use the laser and capacitance displacement sensors to measure the signal, respectively. And then, record the reading and the output voltage, respectively. The experiment data was processed with the criteria of least squares. Curves and equations of linear fitting were obtained, which were shown in Fig.22 and Fig.23. From these two figures, relation between measured

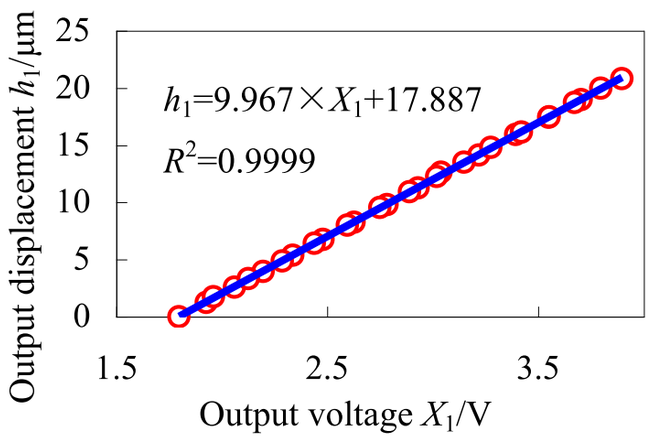

Fig. 22. Calibration curve of the laser displacement sensor

displacement h_1/μm and output voltage X_1/V of the laser displacement sensor was h_1=9.967×X_1-17.887 and relation between measured displacement h_2/μm and output voltage X_2/V of the capacitance displacement sensor was h_2=49.538×X_2−194.27. Their linear correlation coefficients R^2 were both close to 1, which showed the two sensors had high linearity. So the equations of linear fitting can be used in the experiment without correction.

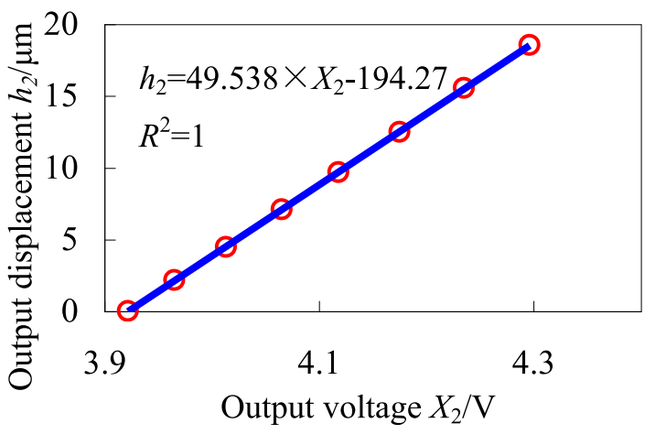

Fig. 23. Calibration curve of the capacitance displacement sensor

7.2 Calibration experiments of the displacement amplification structure

According to section 3, the displacement amplification structure plays an important role in the measuring unit as well as the entire indentation device. Calibration experiments were carried out to obtain the relation of load P and output displacement h_1 of point B as well as the relation of deformation h_3 of point A and output displacement h_1 of point B, and the results were shown in Fig.24 and Fig.25.

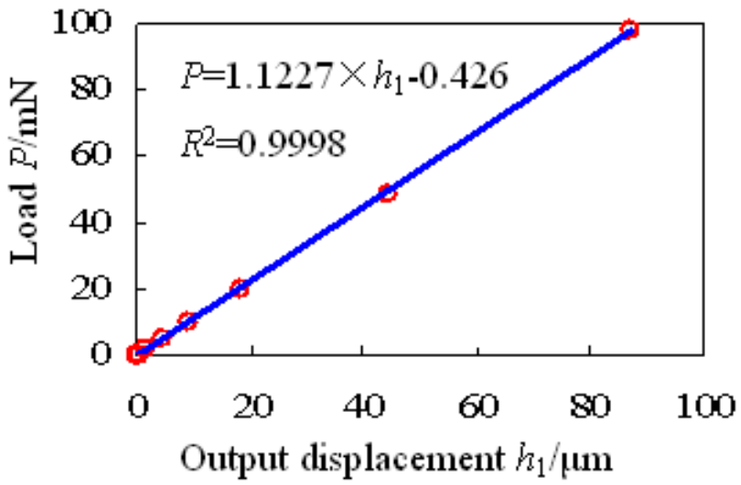

Fig. 24. Relation curve of load P and displacement h_1

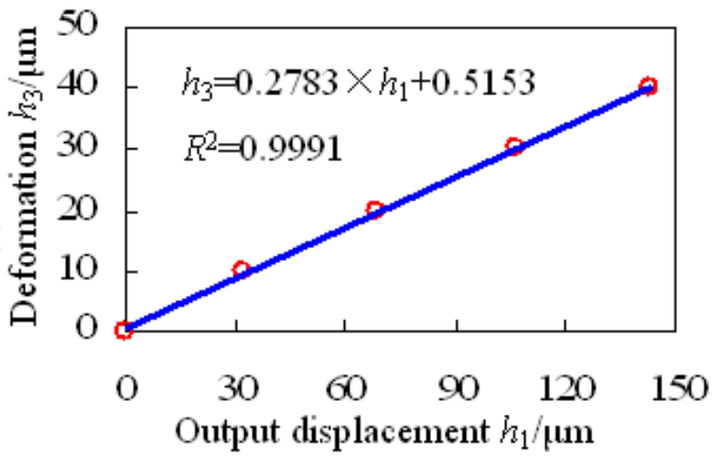

Fig. 25. Relation curve of displacement h_3 and h_1

From these two figures, relation between the load P/mN and output displacement h_1/μm of point B of the displacement amplification structure was P=1.1227Xh_1-0.426, and relation between deformation h_3/μm of point A and output displacement h_1/μm of point B is h_3=0.2783×h_1+0.5153. Their linear correlation coefficients R^2 were 0.9998 and 0.9991, which indicated that output of the structure was linear. Also equations of linear fitting can be used in the experiment without correction.

7.3 Output performance of x-y precise positioning hinge and z-axis precise driving hinge

Output performances of x-y precise positioning hinge and z-axis precise driving hinge were tested by laser displacement sensor. The range of applied voltage was form 0V to 120V for x and y piezoelectric stacks with step of 5V while the range was from 0V to 90V for z axis piezoelectric stack with step of 5V or various steps (5V to 1V). The testing results were shown in Fig.26 - Fig.29.

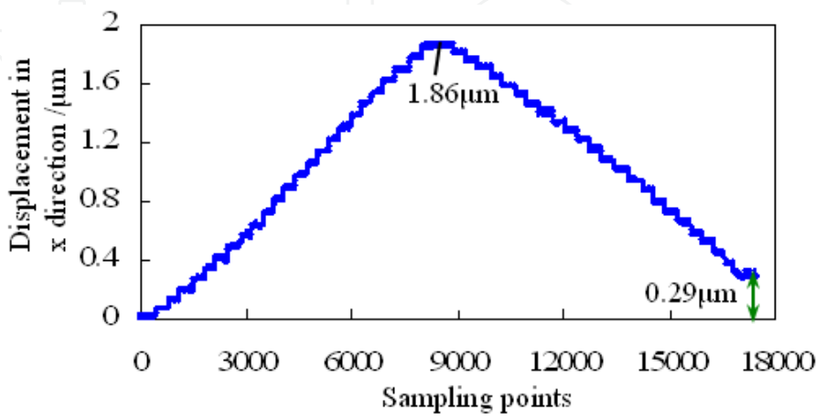

Fig. 26. Output displacement in x direction

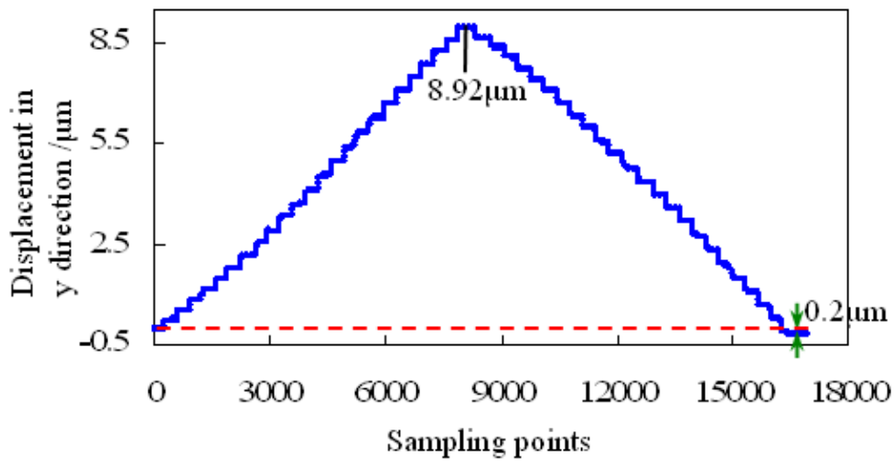

Fig. 27. Output displacement in y direction

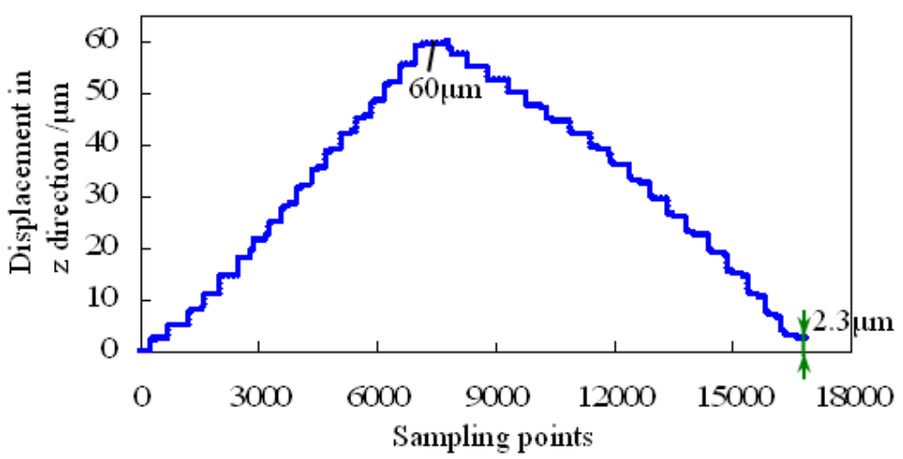

Fig. 28. Output displacement in z direction

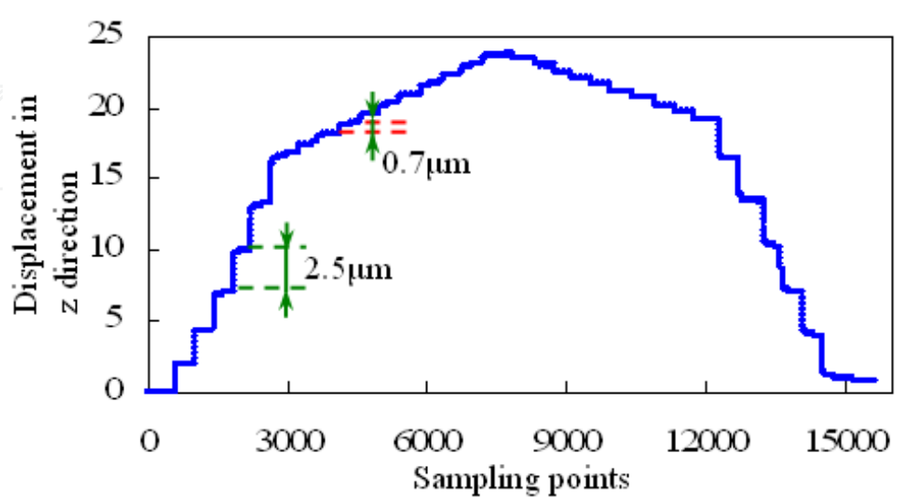

Fig. 29. Output displacement in z direction with various steps

As shown in Fig.26 and Fig.27, the output performances were large different for x and y axis. The maximum output displacement was 1.86μm in x direction while it was 8.92μm in y direction. For 24 steps, the total output displacement was 77.5nm and 371.7nm in x and y directions respectively. So it had different output displacement resolution in the two directions. These differences were caused by different stiffness of flexure hinges in x and y directions.

Fig.28 was the output curve of z-axis precise driving hinge when applied voltage was from 0V to 90V with step of 5V. The maximum output displacement was about 60μm at voltage of 90V, which was large than the maximum output displacement of z piezoelectric stack about 40μm. So the z-axis precise driving hinge had the function of displacement magnification. Fig.29 was the output curve of z-axis precise driving hinge with various steps from 5V to 1V. Due to the hysteresis of piezoelectric stack, the curve was asymmetrical. Through the manner of various steps, it was convenient to realize the judgement of contact between the indenter and the sample with large step and to realize loading and unloading process with small step. Also it can be used to research the mechanical performance of materials under different steps.

In order to evaluate performance of the unit, parameters were defined as follows. D_s was the maximum output displacement. D_r was the residual displacement. β was the absolute error. α was the average error of each step. And then, β and a can be expressed

$$\beta = D_r/D_s \times 100\% \tag{11}$$

$$a = D_r/n \tag{12}$$

where n was the total steps in a test circle.

According to equations (11) and (12), parameters were obtained and listed in Table 4. When the voltage step decreases, higher resolution will be obtained and unlimited resolution will be possible under ideal conditions.

	x axis	y axis	z axis
D_s(μm)	1.86	8.92	60
D_r(μm)	0.29	-0.2	2.3
β	15.6%	2.24%	3.83%
a(nm)	6.04	4.17	63.8
Resolution (μm /5v)	0.0775	0.3717	3.33

Table 4. Parameters of three directions

7.4 Indentation test of optical glass

Indentation experiments of optical glass were carried out and the *P-h* curves were shown in Fig.30 and Fig.31.

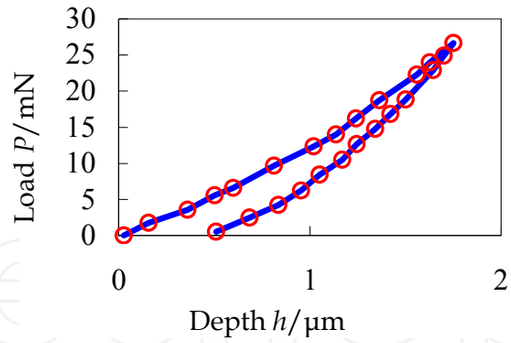

Fig. 30. *P-h* curve with maximum load 26mN

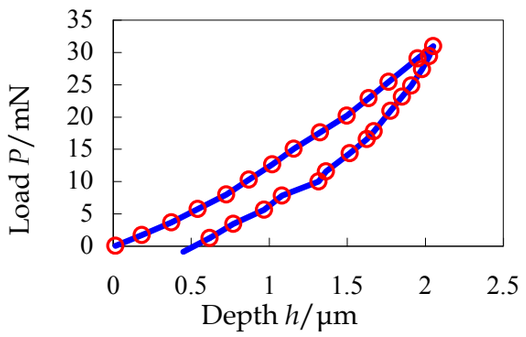

Fig. 31. *P-h* curve with maximum load 30mN

The three polynomial fitting was used to fit the curve of partial unloading data. Fig.32 was fitted curves and equations corresponding to Fig.30, and Fig.33 was fitted curves and equations corresponding to Fig.31. As shown in Fig.32 and Fig.33, the correlation coefficients were close to 1 which indicated that the selected order was suitable. So the relation between load *P* and the depth of partial unloading for the two experiments were given：

Test one with maximum load 26mN: $P= 22.197\times h^3 -85.055\times h^2 + 131.78\times h - 62.456$;

Test two with maximum load 30mN: $P= 107.74\times h^3 - 570.35\times h^2 + 1033.6\times h - 619.31$.

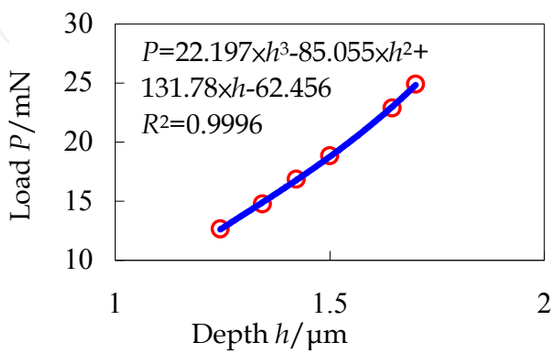

Fig. 32. Fitted curves and equations of partial unloading data of test one

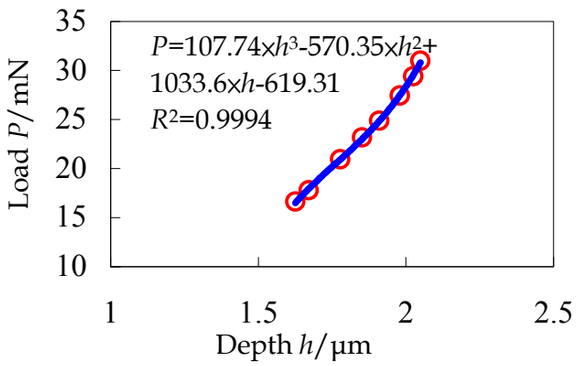

Fig. 33. Fitted curves and equations of partial unloading data of test two

According to equations mentioned in section 2, contact stiffness between indenter and optical glass of the two experiments was 35.0801mN/μm for test one and 53.49705mN/μm for test two. The relation between hardness H and load P at the unloading portion was obtained shown in Fig.34 (test one) and Fig.35 (test two) from which we can see that material's hardness would change with penetration depth but it would stabilise when the depth was larger than a certain value.

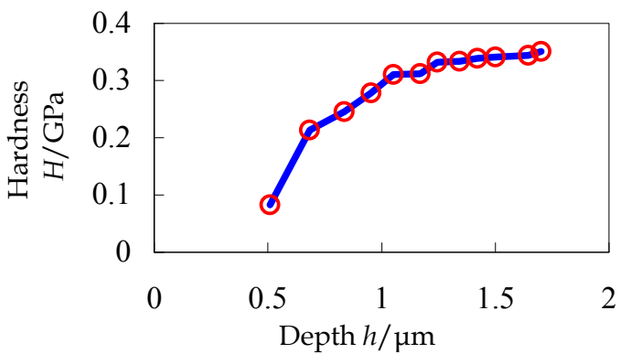

Fig. 34. Relation curve between hardness H and depth h of test one

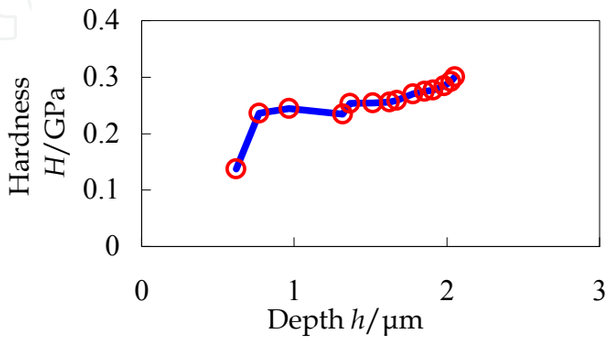

Fig. 35. Relation curve between hardness H and depth h of test two

Compared with the result by commercial indentation device shown in Fig.36 (Zhao et al., 2009), the measured penetration depth was larger at a same load which was caused by structure compliance, indenter installation as well as the sample surface process, and it would be reduced and eliminated in our future work.

The indentation morphology was obtained through high resolution optical microscope shown in Fig.37. The material generated some cracks which had significant value to analyze the damage mechanism especially that the full measuring process was monitored by SEM, TEM as well as other monitoring methods.

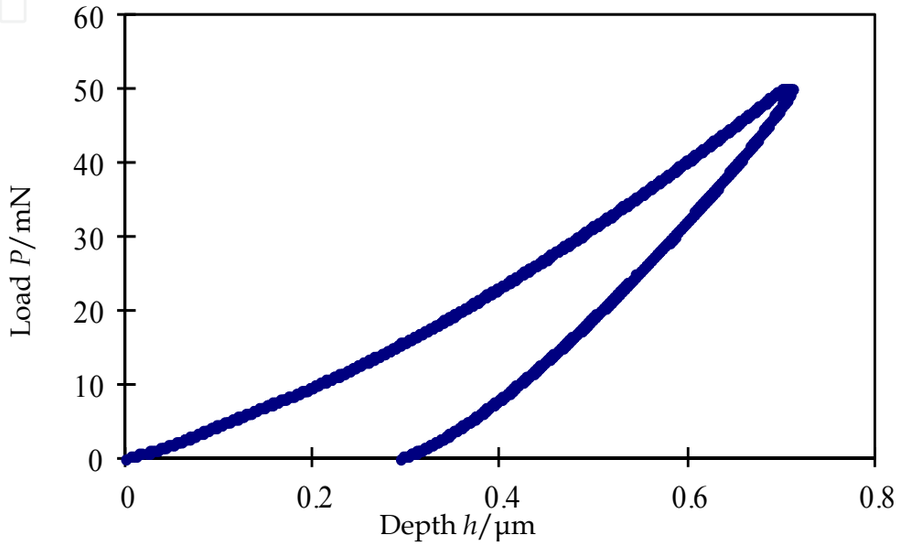

Fig. 36. *P-h* curve obtained from a commercial indentation device

Fig. 37. Indentation morphology of optical glass

The designed indentation device integrating flexure hinges and piezoelectric actuators is smaller than commercial indentation devices but can realize high precise measurement which gives solid foundation for our future work. We will make the device more precise and design smaller indentation device that can be located on the platform of SEM to realize in situ measurement.

8. Conclusions

A new kind of indentation measurement method through two displacement sensors and a displacement amplification structure was proposed and established. Based on this method, a miniaturization indentation device was designed and analyzed. Hysteresis of two kinds of piezoelectric stacks were measured and analyzed. The hysteresis was different for different piezoelectric stacks.

Two key components of the device, the precise driving and precise measuring units, were designed and analyzed. Results from static and modal analysis indicated that designed hinges and amplification structure had enough strength. The dynamic performances of flexure hinges were good but the natural frequencies of the amplification structure were low. So the work frequency of the indentation device should be away from the natural frequencies of the amplification structure to avoid sympathetic vibration and also it is better to take measures to alleviate and isolate the vibration existing in the surroundings.

Calibration experimental results of the two displacement sensors and the amplification structure showed that they all had high linearity. The amplification structure had functions of stage and load-sensing, and can be used to realize precise load measurement.

Output performances of flexure hinges were measured and obtained. They all had stable output displacement and the output resolution was related with the voltage step applied to the piezoelectric stack.

Indentation experiments of optical glass were carried out. Relation curves between load and penetration depth were obtained. Contact stiffness and hardness were discussed. Curves obtained from the designed device and commercial device were compared and analyzed. The designed indentation device had smaller volume and can realize indentation test but the accuracy should be improved more.

The future work will focus on designing smaller indentation device and realizing in situ experiments.

9. Acknowledgements

This research is funded by the National Natural Science Foundation of China (Grant No. 50905073), Research Fund for the Doctoral Program of Higher Education of China (Grant No.200801831024), Research Fund of the Ministry of Science and Technology of China (Grant No.2009GJB10029), Young Scientist Fund of Jilin Province of China (Grant No.20090101), The International Scientific and Technological Cooperation Project (Grant No.2010DFA72000) and Graduate Innovation Fund of Jilin University (Grant No.20111058).

10. Reference

Abdel-Aal, H.A.; Patten, J.A. & Dong, L. (2005). On the thermal aspects of ductile regime micro- scratching of single crystal silicon for NEMS/MEMS applications. *Wear*, Vol.259, No.7-12, (May 2005), pp. 1343-1351, ISSN 0043-1648

Bhushan, B. (2007). Nanotribology and nanomechanics of MEMS/NEMS and BioMEMS/BioNEMS materials and devices. *Microelectron Eng.*, Vol. 84, No.3, (March 2007), pp. 387-412, ISSN 0167-9317

Bradby, J.E.; Williams, J.S. & Swain, M. V. (2003). In situ electrical characterization of phase transformations in Si during indentation. *Phys. Rev. B*, Vol.67, No.8, (February 2003), pp. 085205.(1-9), ISSN 1098-0121

Bruet, B. J. F.; Song, J.H.; Boyce, M.C. & Ortiz, C. (2008). Materials design principles of ancient fish armour. *Nat. Mater.*, Vol. 7, No.9, (July 2008), pp.748-756, ISSN 1476-1122

CSIRO.UMIS. Cited 2011; Available from: http://www.csiro.au/hannover/2000/catalog/projects/umis. Html

CSM instruments. Cited 2011; Available from: www.csm-instruments.com

De Hosson, J.T.M.; Soer, W.A.; Minor, A.M.; Shan, Z.W.; Stach, E.A.; Syed Asif, S.A. & Warren, O.L.(2006). In situ TEM nanoindentation and dislocation-grain boundary interactions: a tribute to David Brandon. *J. Mater Sci.*, Vol.41, No.23, (Novermber 2006), pp.7704-7719, ISSN 0022-2461

Diez-Perez, A.; Güerri, R.; Nogues, X.; Cáceres, E.; Peña, M.J.; Mellibovsky, L.; Randall, C.; Bridges, D.; Weaver, J.C.; Proctor, A.; Brimer, D.; Koester, K.J.; Ritchie, R.O. & Hansma, P.K. (2010). Microindentation for In Vivo Measurement of Bone Tissue Mechanical Properties in Humans. *J. Bone Miner. Res.*, Vol.25, No.8, (August 2010), pp. 1877-1885;

Doerner, M.F. & Nix, W.D. (1986). A method for interpreting the data from depth-sensing indentation instruments. *J. Mater. Res.*, Vol.1, No.4, pp.601-609, (August 1986), ISSN 0884-2914

Han, X.; Zhang, Z. & Wang, Z. (2007). Experimental nanomechanics of one-dimensional nanomaterials by in situ microscopy. *NANO.*, Vol.2, No.5, (October 2007), pp. 249–271, ISSN 1793-2920

Hansma, P.K.; Turner, P. J. & Fantner, G.E. (2006). Bone diagnostic instrument. *Rev. Sci. Instrum.*, Vol.77, No.7, (July 2006), pp. 075105(1-6), ISSN 0034-6748

Hemker, K.J. & Nix, W.D.(2008). Nanoscale deformation: Seeing is believing. *Nat. Mater.*, Vol.7, No.2 (February 2008), pp. 97-98, ISSN 1476-1122

Huja, S.S.; Hay, J.L.; Rumme, A.M. & Beck, F.M. (2010). Quasi-static and harmonic indentation of osteonal bone. *J. Dent. Biomech.*, Vol. 2010, (February 2010), pp. 736830(1-7) , ISSN 1758-7360

Hysitron Incorporated. Cited 2011; Available from: http://www.hysitron.com/

Jardret, V. & Morel, P. (2003). Viscoelastic effects on the scratch resistance of polymers: relationship between mechanical properties and scratch properties at various temperatures. *Prog. Org. Coat.*, Vol.48, No.2-4, (December 2003), pp. 322-331, ISSN 0300-9440

Koff, M.F.; Chong, L.R.; Virtue, P.; Chen, D.; Wang, X.; Wright, T. & Potter, H.G.(2010). Validation of cartilage thickness calculations using indentation analysis. *J. Biomech. Eng.*, Vol.132, No.4, (April 2010), pp. 041007(1-6), ISSN 0148-0731

Lim, C.T.; Zhou, E.H. & Quek, S.T. (2006). Mechanical models for living cells—a review. *J. Biomech.*, Vol.39, No.2, (January 2006), pp. 195-216, ISSN 0021-9290

Lucas, B.N. & Oliver, W.C. (1999). Indentation power-law creep of high-purity indium. *Metall. Mater. Trans. A*, Vol.30, No.3, pp. 601-610, (March 1999), ISSN 1073-5623

Michler, J.; Rabe, R.; Bucaille, J-L.; Moser, B.; Schwaller, P. & Breguet, J-M.(2005). Investigation of wear mechanisms through in situ observation during microscratching inside the scanning electron microscope. *Wear*, Vol.259, (May 2005), pp. 18-26, ISSN 0043-1648

Micro Materials Ltd. Cited 2011; Available from: www.micromatreials.co.uk

MTS NanoIndenter. Cited 2011; Available from: http://www.charfac.umn.edu/InstDesc/nanoindenterdesc.html

Nowak, R.; Chrobak, D.; Nagao, S.; Vodnick, D.; Berg, M.; Tukiainen, A. & Pessa, M. (2009). An electric current spike linked to nanoscale plasticity. *Nat. Nanotechnol.*, Vol. 4, No.5, (March 2009), pp. 287-291, ISSN 1748-3387

Oliver, W.C. & Pharr, G.M. (1992). An improved technique for determining hardness and elastic modulus using load and displacement sensing indentation measurements. *J. Mater. Res.*, Vol.7, No.6, pp.1564-1583, (June 1992), ISSN 0884-2914

Rabe, R. (2006). Compact test platform for in-situ indentation and scratching inside a scanning electron microscope (SEM). PhD thesis, EPFL, 3593 (2006)

Schuh, C.A.; Mason, J.K. & Lund, A.C. (2005). Quantitative insight intodislocation nucleation fromhigh-temperature nanoindentation experiments. *Nat. Mater.*, Vol.4, No.8, (August 2005), pp. 617-621, ISSN 1476-1122

Sneddon I.N. (1965). The relation between load and penetration in the axisymmetric boussinesq problem for a punch of arbitrary profile. Int. J. Eng. Sci., Vol.3, No.1, (May 1965), pp. 47-57, ISSN 0020-7225

Suresh, S.; Spatz, J.; Mills, J.P.; Micoulet, A.; Dao, M.; Lim, C.T.; Beil, M. & Seufferlein, T. (2005). Connections between single-cell biomechanics and human disease states: gastrointestinal cancer and malaria. *Acta. mater.*, Vol. 1, No.1, (January 2005), pp. 15-30, ISSN 1359-6454

Suresh, S. (2007). Nanomedicine: elastic clues in cancer detection. *Nat. Nanotechnol.*, Vol.2, No.12, (December 2007), pp. 748 – 749, ISSN 1748-3387

Tai, K.; Dao, M.; Suresh, S.; Palazoglu, A. & Ortiz, C. (2007). Nanoscale heterogeneity promotes energy dissipation in bone. *Nat. Mater.*, Vol.6, No.6, (May 2007), pp. 454 – 462, ISSN 1476-1122

Tao, P.J.; Yang, Y.Z. & Bai, X.J. (2010). Vickers indentation tests in a Zr62.55Cu17.55Ni9.9Al10 bulk amorphous alloy. *Mater. Lett.*, Vol.64, No.9, (May 2010), pp. 1102-1104, ISSN 0167-577X

Thurner, P.J. (2009). Atomic force microscopy and indentation force measurement of bone. *WIREs Nanomed. Nanobiotechnol.* Vol.1, No.6, (October 2009), pp. 624–649, ISSN 1939-0041

Yang, F.Q.; Geng, K.B.; Liaw, P.K.; Fan, G.J. & Choo, H. (2007). Deformation in a Zr57Ti5Cu20Ni8Al10 bulk metallic glass during nanoindentation. *Acta. mater.*, Vol.55, No.1, pp. 321-327, (January 2007), ISSN 1359-6454

Zhang, J.Z.; Michalenko, M.M.; Kuhl, E. & Ovaert, T.C. (2010). Characterization of indentation response and stiffness reduction of bone using a continuum damage model. *J. Mech. Behav. Biomed. Mater.*, Vol.3, No. 2, (February 2010), pp. 189-202, ISSN 1751-6161

Zhao, H.W.; Yang, B.H.; Zhao, H.J. & Huang, H. (2009). Test of nanomechanical properties of single crystal silicon. *Optics and Precision Engineering*, Vol.17, No.7, (July 2007), pp.1602-1608, ISSN 1004-924X

Zheng, Y.P. & Mak, A.F.T.(1996). An ultrasound indentation system for biomechanical properties assessment of soft tissues in-vivo. *IEEE T. Biomed. Eng.*, Vol. 43, No.9, (April 1996), pp. 912-918, ISSN 0018-9294

Zhou, J. & Komvopoulos, K.(2006). Nanoscale plastic deformation and fracture of polymers studied by in situ nanoindentation in a transmission electron microscope. *Appl. Phys. Lett.*, Vol.88, No.18, (May 2006). pp. 181908 (1-3), ISSN 0003-6951

Zhu, Y. & Espinosa, H.D. (2005). An electromechanical material testing system for in situ electron microscopy and applications. *Proc. Natl. Acad. Sci.*, Vol.102, No.41, (August 2005), pp. 14503– 14508, ISSN 1091-6490

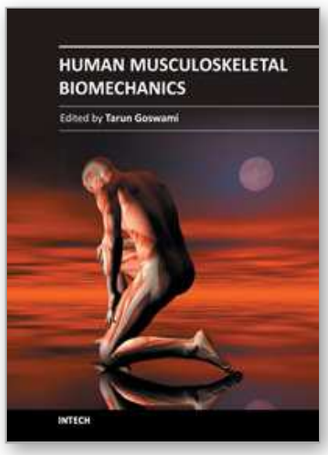

Human Musculoskeletal Biomechanics

Edited by Dr. Tarun Goswami

ISBN 978-953-307-638-6
Hard cover, 244 pages
Publisher InTech
Published online 05, January, 2012
Published in print edition January, 2012

This book covers many aspects of human musculoskeletal biomechanics. As the title represents, aspects of forces, motion, kinetics, kinematics, deformation, stress, and strain are examined for a range of topics such as human muscles, skeleton, and vascular biomechanics independently or in the presence of devices. Topics range from image processing to interpret range of motion and/or diseases, to subject specific temporomandibular joint, spinal units, braces to control scoliosis, hand functions, spine anthropometric analyses along with finite element analyses. Therefore, this book will be valuable to students at introductory level to researchers at MS and PhD level searching for science of specific muscle/vascular to skeletal biomechanics. This book will be an ideal text to keep for graduate students in biomedical engineering since it is available for free, students may want to make use of this opportunity. Those that are interested to participate in the future edition of this book, on the same topic, as a contributor please feel free to contact the author.

How to reference

In order to correctly reference this scholarly work, feel free to copy and paste the following:

Hongwei Zhao, Hu Huang, Jiabin Ji and Zhichao Ma (2012). Design and Analysis of Key Components in the Nanoindentation and Scratch Test Device, Human Musculoskeletal Biomechanics, Dr. Tarun Goswami (Ed.), ISBN: 978-953-307-638-6, InTech, Available from: http://www.intechopen.com/books/human-musculoskeletal-biomechanics/design-and-analysis-of-key-components-in-the-nanoindentation-and-scratch-test-device

INTECH
open science | open minds

InTech Europe
University Campus STeP Ri
Slavka Krautzeka 83/A
51000 Rijeka, Croatia
Phone: +385 (51) 770 447
Fax: +385 (51) 686 166
www.intechopen.com

InTech China
Unit 405, Office Block, Hotel Equatorial Shanghai
No.65, Yan An Road (West), Shanghai, 200040, China
中国上海市延安西路65号上海国际贵都大饭店办公楼405单元
Phone: +86-21-62489820
Fax: +86-21-62489821

IntechOpen